Available online at www.sciencedirect.com
SCIENCE DIRECT
Journal of Asian Earth Sciences 27 (2006) 805–818
Journal of Asian Earth Sciences
www.elsevier.com/locate/jaes

A stable isotope and fluid inclusion study of the Qaleh-Zari Cu–Au–Ag deposit, Khorasan Province, Iran

Ali A. Hassan-Nezhad [a], Farid Moore [b,*]

[a] College of Earth Sciences, Damghan University of Basic Sciences, Damghan, Iran
[b] Department of Earth Sciences, College of Sciences, Shiraz University, Shiraz, Iran

Received 6 August 2004; accepted 26 August 2005

Abstract

The Qaleh-Zari copper deposit, located in South Khorasan in the Central Lut region of Iran, is a polymetallic vein deposit with major amounts of Cu, Au, Ag and minor amounts of Pb, Zn and Bi. Mineralization occurs in a series of NW–SE trending fault planes and breccia zones in Paleogene andesitic to basaltic volcanic rocks. Argillization, sericitization and propylitization characterize alteration halos bordering mineral veins. The main ore minerals are chalcopyrite, pyrite, galena and sphalerite, with quartz, calcite and minor chlorite as the main gangue phases. Microthermometric measurements of fluid inclusions in cogenetic quartz indicate homogenization temperatures between 160 and 300 °C and salinities from 1 to 4 wt% NaCl equiv. Boiling occurred in the mineralising fluids at 160–1000 m below the paleo-water table at pressures of approximately 15–80 bar at various stages in the formation of the ore body. The wide range of pressures and temperatures reflects the multi-stage nature of the mineralization at Qaleh-Zari. The $\delta^{18}O$ values in quartz (relative to SMOW) and $\delta^{34}S$ values in chalcopyrite and galena (relative to CDT) range from 6.5 to 7.5‰ and 0.0–1.5‰ (mean: 7.0‰), respectively. At 300 °C, calculated fluid $\delta^{18}O$ values are close to 0‰. These data suggest a magmatic origin for sulfur and a surficial origin for the mineralizing fluid. Mineralization at Qaleh-Zari is interpreted as epithermal and low-sulfidation in style and was probably related to a deep-seated magmatic system. Ore deposition was the result of boiling, cooling and pressure reduction.

1. Introduction

Iran is located on the Tethyan Copper Belt, and has a long history of copper mining and smelting dating back to 9000BP (Joseph, 1999). To date more than 500 ore bodies and showings have been identified (Khoie et al., 1999).

Bazin and Hubner (1969) suggested that copper ore deposits in Iran occur in five geographic zones; North Azarbaijan, Tarom, Anarak, Abasabad and Kerman regions. A recent study (Khoie et al., 1999) identifies the following six zones as the main locations of copper mineralization in Iran (Fig. 1): 1. Orumieh-Dokhtar Belt; 2. Western Alborz Zone; 3. Kavir-Sabzevar Zone; 4. Sabalan; 5. Lut area; 6. Makran area. The Orumieh-Dokhtar Belt is the most important for copper, and hosts the majority of the larger porphyry copper deposits, including Sar Cheshmeh and Meiduk.

The Qaleh-Zari deposit (58°55′15″E, 31°49′ 4″N) is located in the central Lut region, 180 km southwest of Birjand city (Fig. 1). It is a vein-type deposit. Here, mineralization occurs along a series of faults and breccia zones trending NW–SE and dipping 80 to 85° NE or SW. The veins vary in width from 0.5 to 10 m and in addition to copper, silver and gold contain elevated concentrations of Fe, Pb, Zn, Te and Bi. Copper grades are between 0.5 and 8 wt%, whilst maximum gold and silver grades are 180 and 600 g/t, respectively (Suzuki et al., 1976).

Copper mining in the Qaleh-Zari region goes back to ancient times. Historic remains show that primitive mining was mainly restricted to the surface, but locally followed some rich veins to depths of up to 70 m. Recent underground mining, jointly by the Iranian Lut Company and the Japanese Titso Company, started in 1970. Currently, Qaleh-Zari is owned and mined by the Iranian Mina Kan mining company. Three major veins are being exploited at different depths via seven shafts, to a maximum depth of 240 m.

In this paper, we present fluid inclusion, stable isotope, petrographic and mineralogic data building on previous studies (Sadaghyani-Avval, 1976; Moore and Hassan-Nezhad, 1994; Karimpour and Zaw, 2000), which enable

* Corresponding author. Tel./fax: +98 711 2284572.
E-mail address: moore@geology.susc.ac.ir (F. Moore).

1367-9120/$ - see front matter © 2005 Published by Elsevier Ltd.
doi:10.1016/j.jseaes.2005.08.002

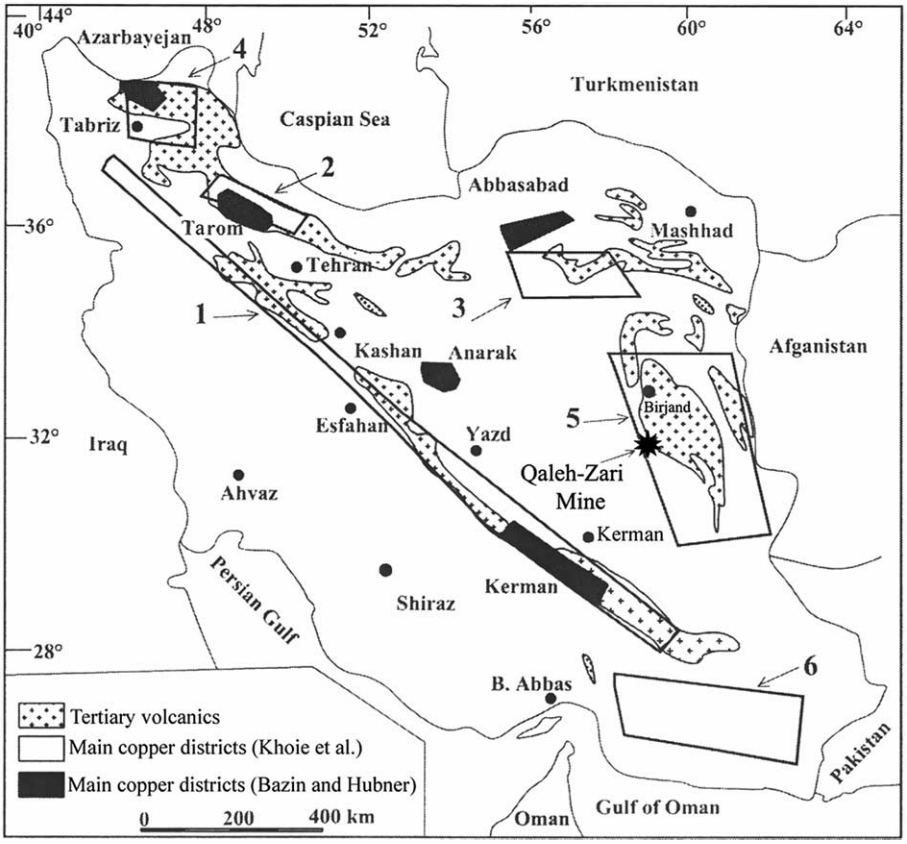

Fig. 1. The main zones of copper mineralization in Iran: (1) Orumieh-Dokhtar Belt; (2) Western Alborz Zone; (3) Kavir-Sabzevar Zone; (4) Sabalan; (5) Lut area; (6) Makran area.

us to present a new interpretation of the genesis of the Qaleh-Zari deposit.

2. Geology

The geology of the Qaleh-Zari area is illustrated in Fig. 2. Sedimentary rocks are the oldest formations in the area and comprise Jurassic shales and sandstones overlain unconformably by Upper Cretaceous red conglomerates (Daymehvar, 1996). Sadaghyani-Avval (1976) also reports localized Jurassic radiolarian cherts and Maestrichtian carbonates. Paleogene volcanic rocks consist of high potassium calc-alkaline andesites (subduction zone shoshonites), andesitic basalts, dacites and rhyolites, andesitic and dacitic tuffs and pyroxene-bearing andesites (Sadaghyani-Avval, 1976; Suzuki et al., 1976; Hassan-Nezhad, 1994). Oligo-Miocene microgranodioritic rocks intrude the volcanic and sedimentary rocks. Mineralization in the Qaleh-Zari area occurs along NW–SE trending fault planes and breccia zones in Paleogene andesitic to basaltic volcanic rocks (Bazin and Hubner, 1969).

3. Structure

The Qaleh-Zari deposit is a fissure-filling polymetallic vein system formed by hydrothermal solutions circulating through fault planes and breccia zones (Sadaghyani-Avval, 1976; Suzuki et al., 1976; Moore and Hassan-Nezhad, 1994; Karimpour and Zaw, 2000). According to Khatib (1999), mineralization in this area occurs in a NW–SE trending transtensional fault system. Faults and fractures can be grouped into the following orientations:

1. NW – SE, these right-lateral high angle faults (dipping about 86°) host the main ore-bearing veins. Dilation in these faults sometimes reaches up to 70 cm.
2. NE – SW, these barren fractures are younger than the other faults and fractures and show left-lateral movement. Locally, these fractures are seen to cut and displace ore-bearing veins, which occur along the oldest faults.
3. N – S, these fractures are the least common. Mineralization along these fractures is very poor and there is no evidence of mining along them. At the surface they are mostly mineralized by quartz and hematite.
4. E – W, faults from the point of view of mineralization are similar to Group 1 faults. In addition, most veins in No.2 deposit (Fig. 2) trend E – W.

The N–W and N–S trending faults cut the NW–SE ones. Textures in the ore minerals show evidence of repeated faulting, fracturing and ore deposition.

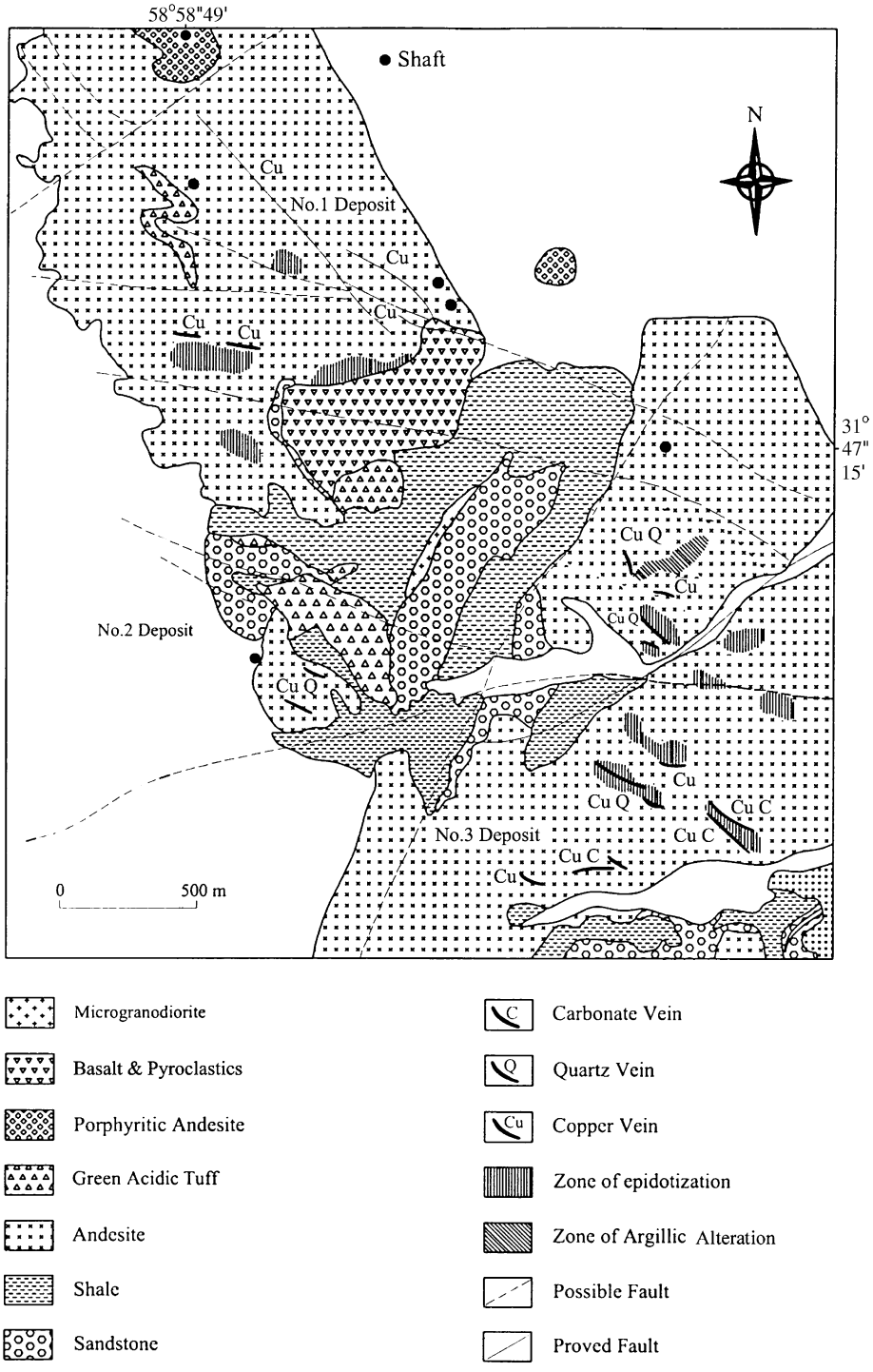

Fig. 2. Simplified geological map of the Qaleh-Zari area (modified after Suzuki et al., 1976).

4. Hydrothermal alteration and mineralization

4.1. Alteration

Four types of hydrothermal alteration are developed in the Qaleh-Zari wall rocks: 1. sericitization; 2. argillization; 3. propylitization; and 4. silicification. Sericite is present as fine-grained aggregates within altered andesitic rocks, especially surrounding and in the cores of plagioclase phenocrysts. Argillic minerals occur in silicified argillic haloes following surficial mineralized veins (kaolinite is identified by XRD analysis). Propylitic alteration is so pervasive that, locally, the host rocks are completely altered to an assemblage of epidote, chlorite, carbonates and pyrite, giving the rock a characteristic green color. Some veins are formed of massive silica, veinlets show mosaic-texture and vugs show comb-structures. The spatial relationships between the various types of alteration is different at the surface and at depth. On the surface the argillic

assemblage is flanked outward by sericitic and propylitic assemblages until fresh rock is reached, while at depth a sericitic assemblage is flanked outward by a propylitic assemblage, but an argillic assemblage does not occur. Tourmaline occurs in the altered rocks, small grains of tourmaline being present mostly in the cores of altered plagioclase crystals.

Supergene effects, with the penetration of surface waters along faults and fractures has led to the oxidation and leaching of the host rocks and the enrichment of copper. Covellite, digenite and chalcocite are located at shallow depths, and in some veins oxidation minerals such as iron hydroxide, azurite, malachite, cuprite and native copper are found extending from the surface to a depth of 70 m.

4.2. Mineralization

Hydrothermal mineralization occurs as an open-space fillings along fault planes, and as a stockwork in the host rocks. Vein thickness ranges from about 20 to 10 m at fault and breccia zone intersections, and the veins extend to depths of at least 250 m below the present-day surface (Fig. 3(a)). The veins display many cavity-filling textures, such as symmetric banding, comb structures and cockade texture (Fig. 3(b)).

Ore and gangue minerals comprise oxide (hematite), sulfide (chalcopyrite, pyrite, galena and sphalerite), sulfosalt (aikinite and matildite), carbonate (calcite) and silicate (quartz and chlorite) minerals. Quartz crystals were deposited as layers in crustification banding and comb structures along the walls of veins or cavities, in response to changes in the environment or the composition of the mineralizing fluids.

The general paragenesis of the mineralization at Qaleh-Zari is illustrated in Fig. 4. In terms of hypogene ore minerals, hematite was the earliest to be deposited and occurs in scaly and lamellar (specularite) forms. Sulfosalts (aikinite group and matildite) are of a similar age, and occur as platy crystals between hematite laths, acting as a host to silver (Fig. 3(c)). The main ore mineral is chalcopyrite. This usually shows a massive texture. It is replaced locally by pyrite, which occurs as euhedral crystals (Fig. 3(d)). The last ore minerals to form,

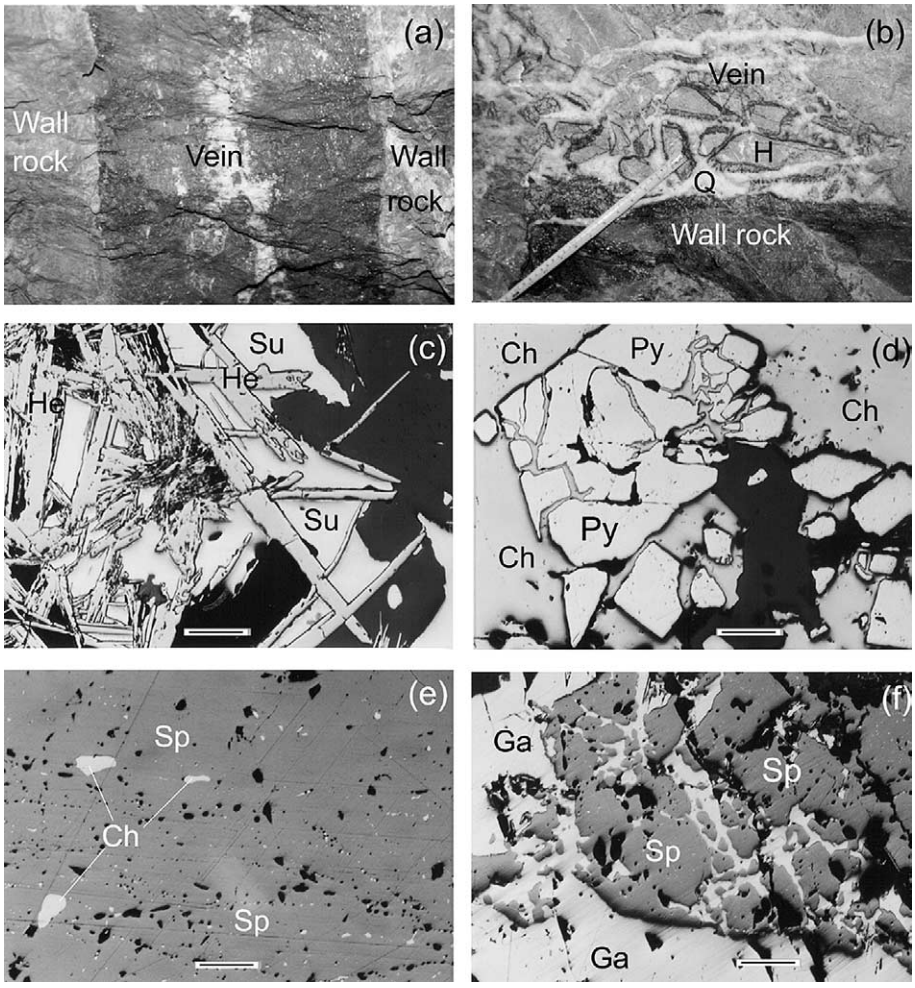

Fig. 3. (a) Photograph of a mineralized vein with a width of about 60 cm within altered andesitic host rock (white minerals are quartz and dark ones are other hydrothermal minerals such as hematite, chalcopyrite, pyrite and chlorite); (b) Photograph of cockade structure showing breccia fragments of host rock with hematite rim (dark) within a ground mass of quartz (Q); (c) Photomicrograph of box-work texture showing hematite lathes (He) and sulfosalt minerals (Su); (d) Photomicrograph of cataclastic texture, pyrite (Py), chalcopyrite (Ch); (e) Photomicrograph of exsolution texture, chalcopyrite blebs (Ch) in sphalerite (Sp); (f) Photomicrograph of replacement texture, galena (Ga), sphalerite (Sp). The scale bar in photomicrographs is 100 μm.

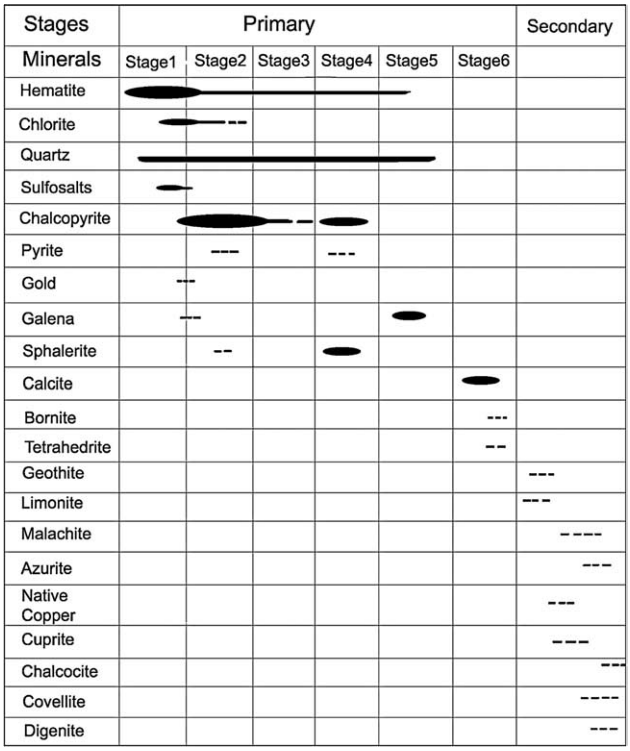

Fig. 4. Schematic diagram showing generalized paragenetic sequence at the Qaleh-Zari ore deposit. The thickness of the horizontal bars indicate the relative abundance of the minerals.

were the base metal sulphides, sphalerite and galena. Sphalerite forms an exsolution texture with chalcopyrite (Fig. 3(e)). There are two generations of galena. The first occurs as solid inclusions in chalcopyrite (Stage 2) while the second-generation forms massive galena (Stage 5) and replaces chalcopyrite and sphalerite (Fig. 3(f)). Tetrahedrite and bornite are of minor occurrence, and are associated with the late base metal sulphide mineralization. Gold occurs as electrum (Suzuki et al., 1976) and is associated with chalcopyrite and hematite.

Evidence of microscopic textures and field observations show that the hypogene minerals at Qaleh-Zari were deposited in a multistage system. Supergene minerals comprise iron-hydroxides, malachite, azurite, native copper, covellite, digenite and chalcocite formed by the weathering of hypogene minerals such as pyrite and chalcopyrite.

5. Fluid inclusions

Previous studies of fluid inclusions in the Qaleh-Zari deposit include those by Sadaghyani-Avval (1976); Moore and Hassan-Nezhad (1994) and Karimpour and Zaw (2000). These workers present information on temperature and chemical conditions of mineral-forming processes in mining levels which are located between No. 1 and No. 2 shafts at depths up to 205 m (below the present-day surface). The studies suggest a temperature range of 130–390°C and salinity of 0.4–2 equiv wt% for the mineralizing fluid. In addition, strong oxidation conditions, high Na/K and very high Na/Mg ratios are suggested for Qaleh-Zari hydrothermal fluid. The present work includes results from mining levels in all the shafts.

5.1. Methods of investigation

Approximately 100 quartz specimens were collected from five production shafts along three major mineralized veins for microthermometric analysis. The samples were collected from different mining horizons at −50, −80, −100, −135, −170, −205 and −240 m from the surface (Fig. 5). Doubly polished wafers were prepared using the procedure of Shepherd et al. (1985). The thickness of the wafers varied between 100 and 300 μm, depending upon the transparency of the quartz crystals.

Microthermometric measurements were made using a Linkam HFS91 combined heating and freezing stage with a temperature range of −196 to 600 °C, mounted on a BH2

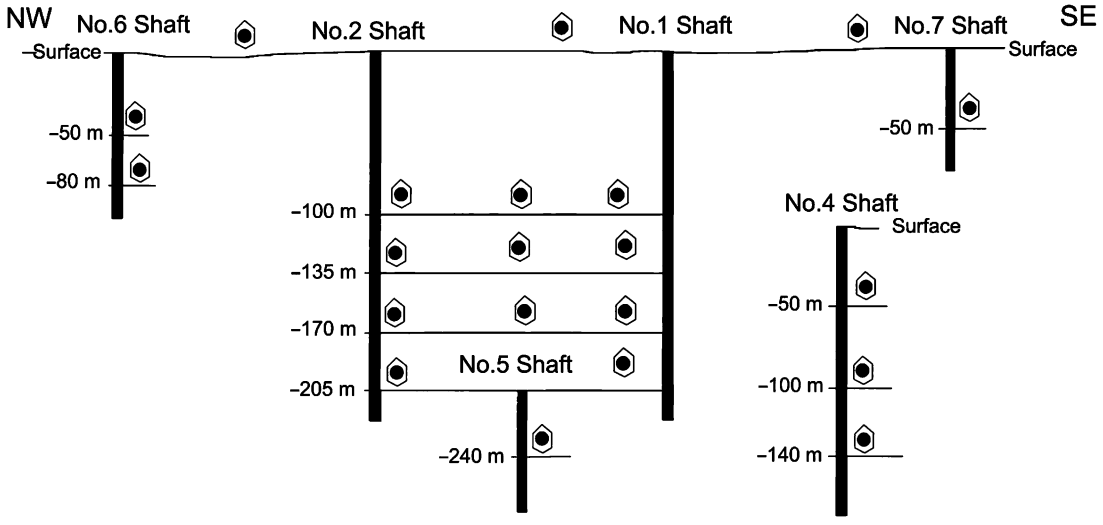

Fig. 5. Six shafts of the Qaleh-Zari ore deposit showing the sampling horizons for fluid inclusion microthermometry.

Olympus petrographic microscope equipped with the Leitz UMK 50/ 0.60, UMK 32/ 0.60 and UM 20/ 0.33 objectives. The melting points of benzoic acid (122 °C), potassium nitrate (335 °C), and potassium dichromate (398 °C) were used for heating calibration, while deionized distilled water (triple point = 0 °C), carbon tetrachloride (triple point = −22.8 °C) and chloroform (triple point = −63.5 °C) were used for freezing calibration. The reported heating and freezing temperatures were reproducible to within ±5 °C (*T*(100 °C) and ±0.1 °C (*T*(50 °C).

5.2. Fluid inclusion petrography

The morphology and petrographic characteristics of the fluid inclusions were recorded at room temperature using the criteria of Roedder (1984); Shepherd et al. (1985). The inclusions vary in size from 5 to 130 μm. Morphologically, the inclusions may be classified by their shape: platy, rod-shaped or negative crystals. Here, inclusions are classified, on the basis of host mineral occurrence, their relationship to each other and the type of inclusion. With respect to their relationship to the host mineral they are classified as primary (isolated inclusions, as well as those in growth zones), secondary (inclusions occurring along fractures that intersect the crystallographic surfaces) and pseudosecondary (inclusions occurring along fractures that do not intersect the crystallographic surfaces). From the relationship of inclusions to each other, they are classified as isolated individual inclusions (Fig. 6(a)), clustering (Fig. 6(b)) or healed fractures and trails (Fig. 6(c)). Some original long tubular inclusions formed in healed cracks show evidence of 'necking down' (Fig. 6(d)) reducing the high surface energy of the inclusion.

5.3. Inclusion types

Based on microthermometric and petrographic studies and the phases that are present, inclusions are divided into (Fig. 7):

I. Monophase liquid inclusions (aqueous liquid).

II. Monophase gaseous inclusions.

III. Two-phase liquid and gas (aqueous liquid + vapour).

IV. Rare carbonic inclusions (aqueous liquid + carbonic phase [L_{CO2} or $L_{CO2} + V_{CO2}$]).

Inclusions types I–III locally trap crystallites of chlorite + hematite, as these two minerals are common in the host quartz (Fig. 7(f)). Type III is the most abundant inclusion type and accounts for 97% of the inclusion population. CO_2-bearing inclusions (Type IV) are extremely rare and only two occurrences have been recorded at Qaleh-Zari.

5.4. Microthermometry

5.4.1. Homogenization temperature (T_h)

Thermometric analyses were performed principally on Type III fluid inclusions which were relatively large ((5 μm) and regular in shape. In addition, primary fluid inclusions, which did not show any evidence of necking down, were selected for microthermometric analyses (Roedder, 1984). Homogenization temperatures of more than 1100 inclusions were measured, and ranging from 150 to 388 °C, with an average of 280 °C. The majority of the inclusions homogenized to a liquid phase (L + V(L). Dew point homogenization (L + V(V)

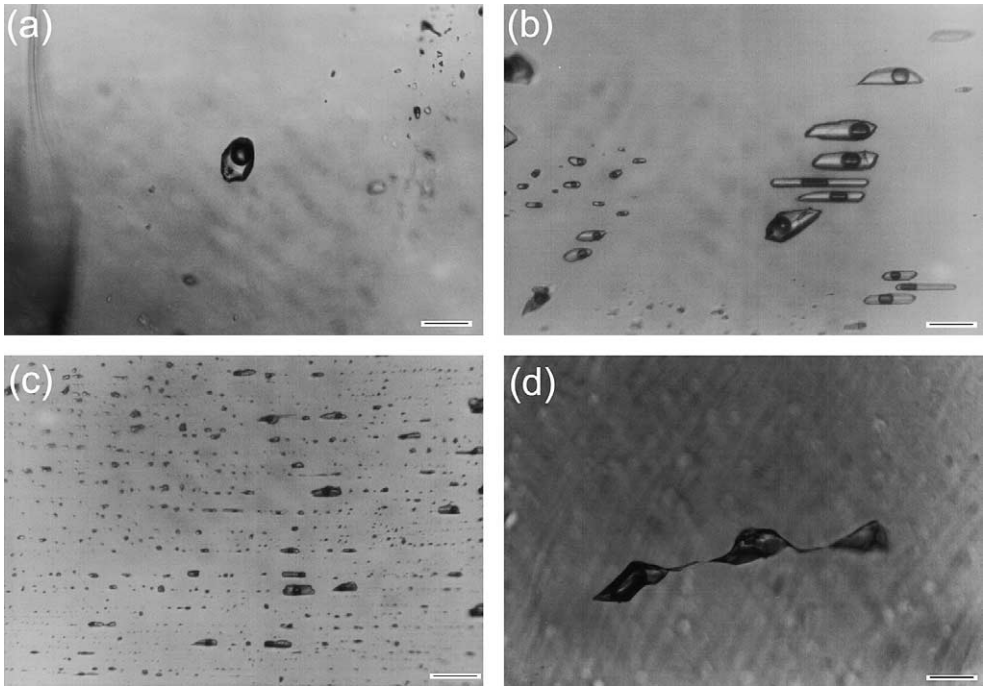

Fig. 6. Photomicrographs showing the distribution pattern of fluid inclusions in quartz from Qaleh-Zari deposit (crossed nicols): (a) Isolated fluid inclusion; (b) Clustering fluid inclusions; (c) Trailed fluid inclusions along sealed microfractures (pseudosecondary fluid inclusions); (d) Necking-down. The scale bar in all photographs is 30 μm.

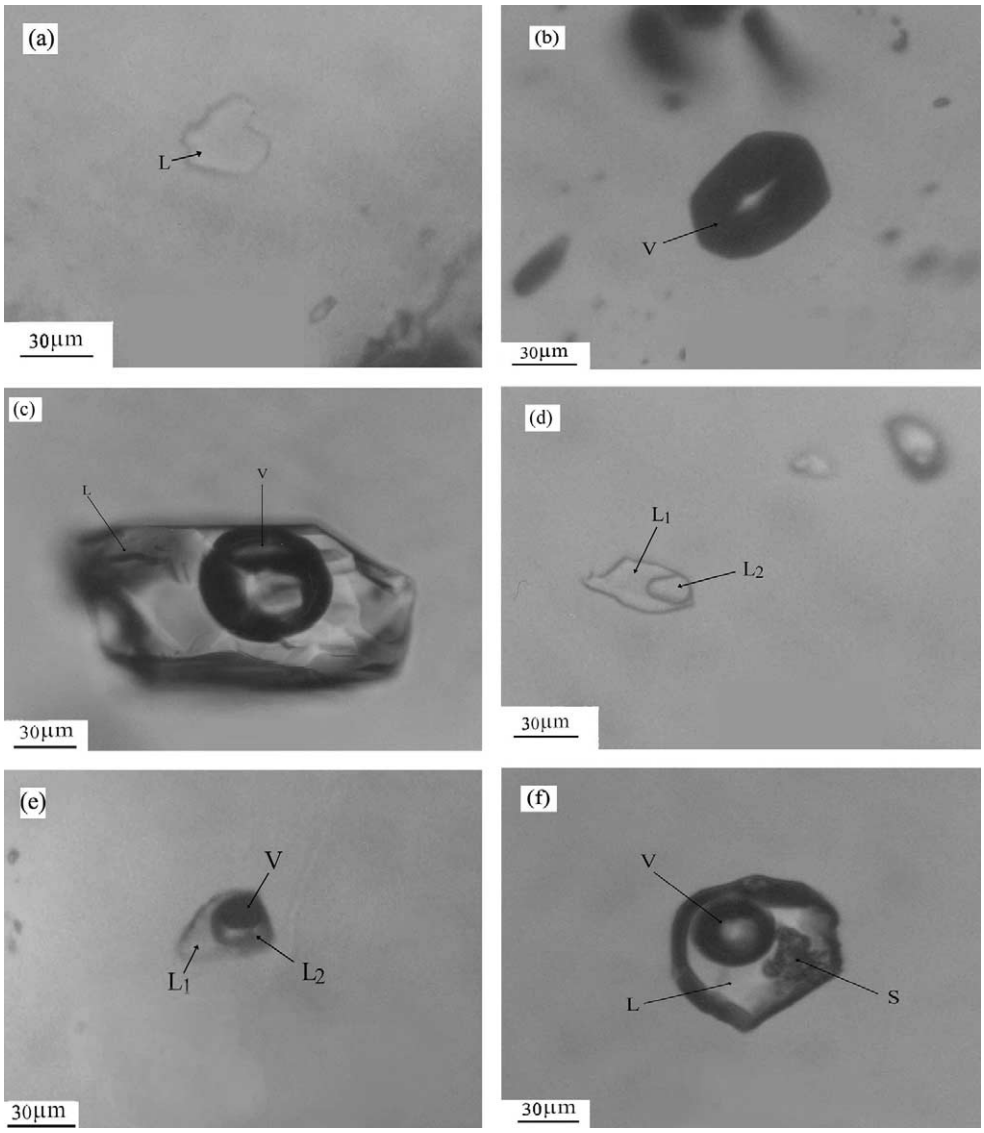

Fig. 7. Photomicrographs of different fluid inclusions in quartz from different horizons at Qaleh-Zari (crossed nicols): (a) fluid inclusions with monophase aqueous liquid (L); (b) fluid inclusions with monophase vapor (V); (c) two phases fluid inclusion, aqueous liquid (L) and a vapor phase (V); (d) two-phase fluid inclusions aqueous liquid (L1) and a CO_2 liquid (L2); (e) three-phase fluid inclusions aqueous liquid (L1), CO_2 liquid (L2) and vapor (V); (f) three-phase fluid inclusions aqueous liquid (L), trapped phase (S, probably chlorite) and a vapor bubble (V).

was rare, and occurred between 365 to 388 °C (mean = 375 °C, $n = 9$). The distribution of this data, based on depth at 50 m intervals, is illustrated in Fig. 8. Histograms of homogenization temperatures show a slight decrease in T_h from depth to the surface, but there is no significant difference in T_h at different horizons. Also, the distribution of data at the lower levels (such as −200 and −250 m) could represent three discrete populations related to the evolution of the mineralizing fluid. No pressure corrections were applied for the T_h values because boiling occurred in the Qaleh-Zari system (Ronacher et al., 2004).

Limited homogenization data were also obtained for post-ore calcite (barren stage) and range from 197 to 256 °C (mean = 230 °C, $n = 32$). Determinations made on secondary inclusions in quartz show that the homogenization temperatures are very close to those in calcite.

5.4.2. Last ice-melting temperature (T_m)

Last ice-melting temperatures of 650 fluid inclusions (Type III) were determined and ranged between −0.5 and −5.8 °C (1.4–7.6 wt% NaCl equiv). Eutectic temperatures of the inclusions vary between −20 and −22 °C, with the exception of eutectic temperatures of four inclusions which gave results between −50 and −50.8 °C. The equation of Bodnar (1993) was used to calculate salinity. The majority of the fluid inclusions (95.8%) displayed salinities between 0.9 and 4.2 wt% NaCl equiv. During determination of the last ice-melting points, only one inclusion (Type III), with a melting temperature of +2.9 °C displayed evidence of clathrate formation. In two inclusions, where liquid CO_2 was observed, T_{mCO2} occurred at −56.4 and −57.6 °C. Homogenization of the CO_2 phase to the liquid phase was between +26.5 and +29.4 °C. The distribution of melting temperatures with

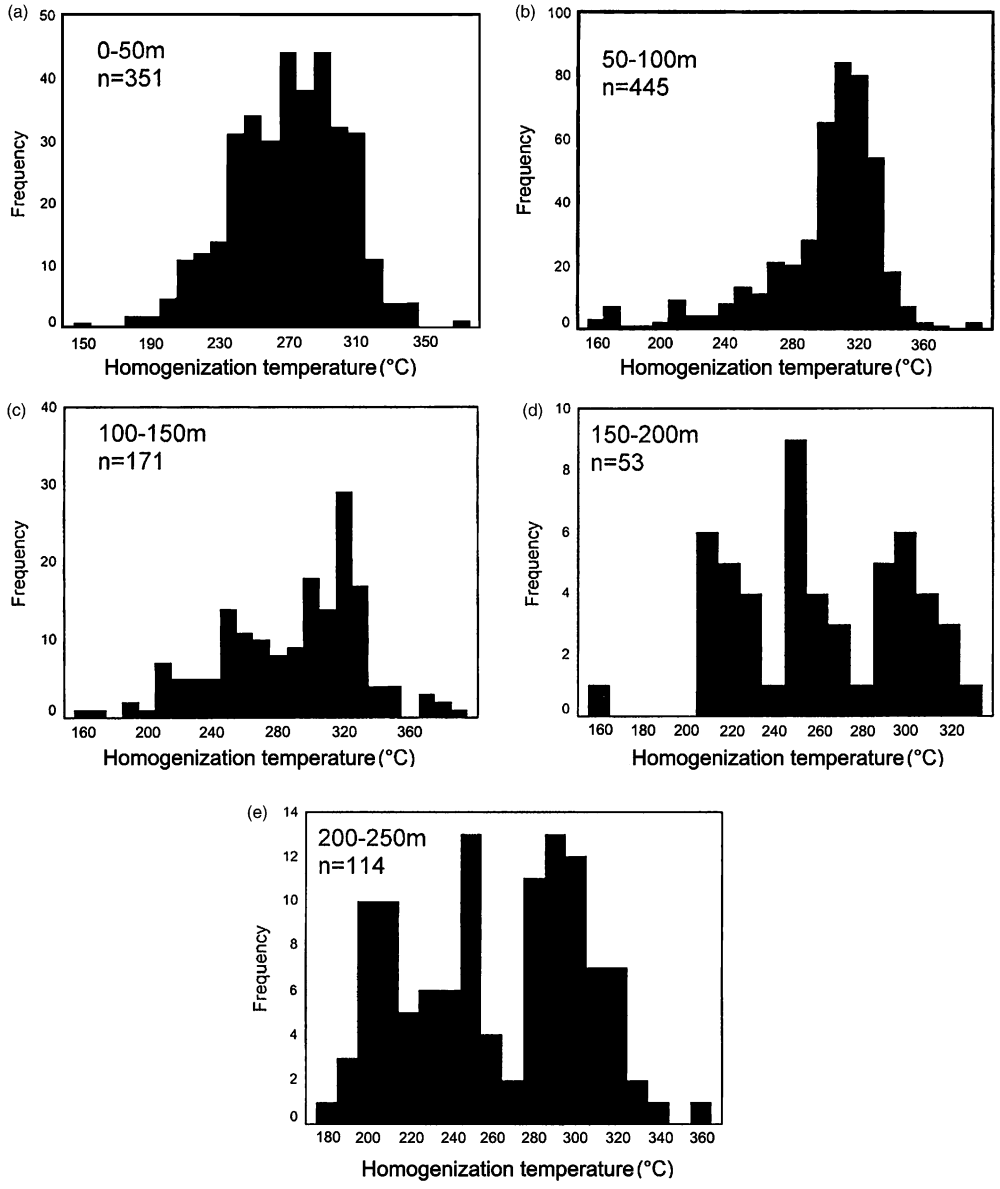

Fig. 8. Distribution of homogenization temperatures for aqueous fluid inclusions: (a) from 0 to 50 m depth; (b) from 50 to 100 m depth; (c) from 100 to 150 m depth; (d) from 150 to 200 m depth; and (e) from 200 to 250 m depth.

depth, at intervals of 50 m, is illustrated in Fig. 9. The largest range in melting temperatures was observed in samples between 100 to 150 m depth (Fig. 9(c)). The eutectic temperatures of the majority of the fluid inclusions indicate that the mineralizing fluid was of H_2O–NaCl type. In contrast, the eutectic temperatures of the secondary fluid inclusions indicate that the post-ore fluid was of H_2O–$CaCl_2$–$MgCl_2$ type (Shepherd et al., 1985).

6. Stable isotopes

Preparation and analysis of quartz and sulfide minerals for oxygen and sulfur isotopes was undertaken at the Scottish Universities Environmental Research Centre using the methods recommended by Macaulay et al. (2000). The $\delta^{18}O$ values for nine analyzed quartz samples (relative to V-SMOW), collected from different horizons of the Qaleh-Zari deposit, range from 6.5 to 7.5‰ (Table 1), with an average of 7‰ and standard deviation of $\pm$0.4‰ (one sigma). The analytical precision of $\delta^{18}O_{quartz}$ is 0.1‰.

Oxygen isotopic composition of hydrothermal water in equilibrium with quartz was calculated using the mean value of an individual homogenization temperature (280 °C) and the mean homogenization temperature of same samples (Table 1) using the fractionation equation of Matsuhisa et al. (1979).

$\delta^{34}S$ values were determined for eight chalcopyrite and two galena specimens relative to V-CDT from different horizons (-240, -170, -140, -100, -80, -50 m) at the Qaleh-Zari mine. The measured values range from 0.0 to 1.6‰ for chalcopyrite (average of 0.6‰) and from 0.3 to 1.5‰ for the two-galena samples. The analytical precision (standard

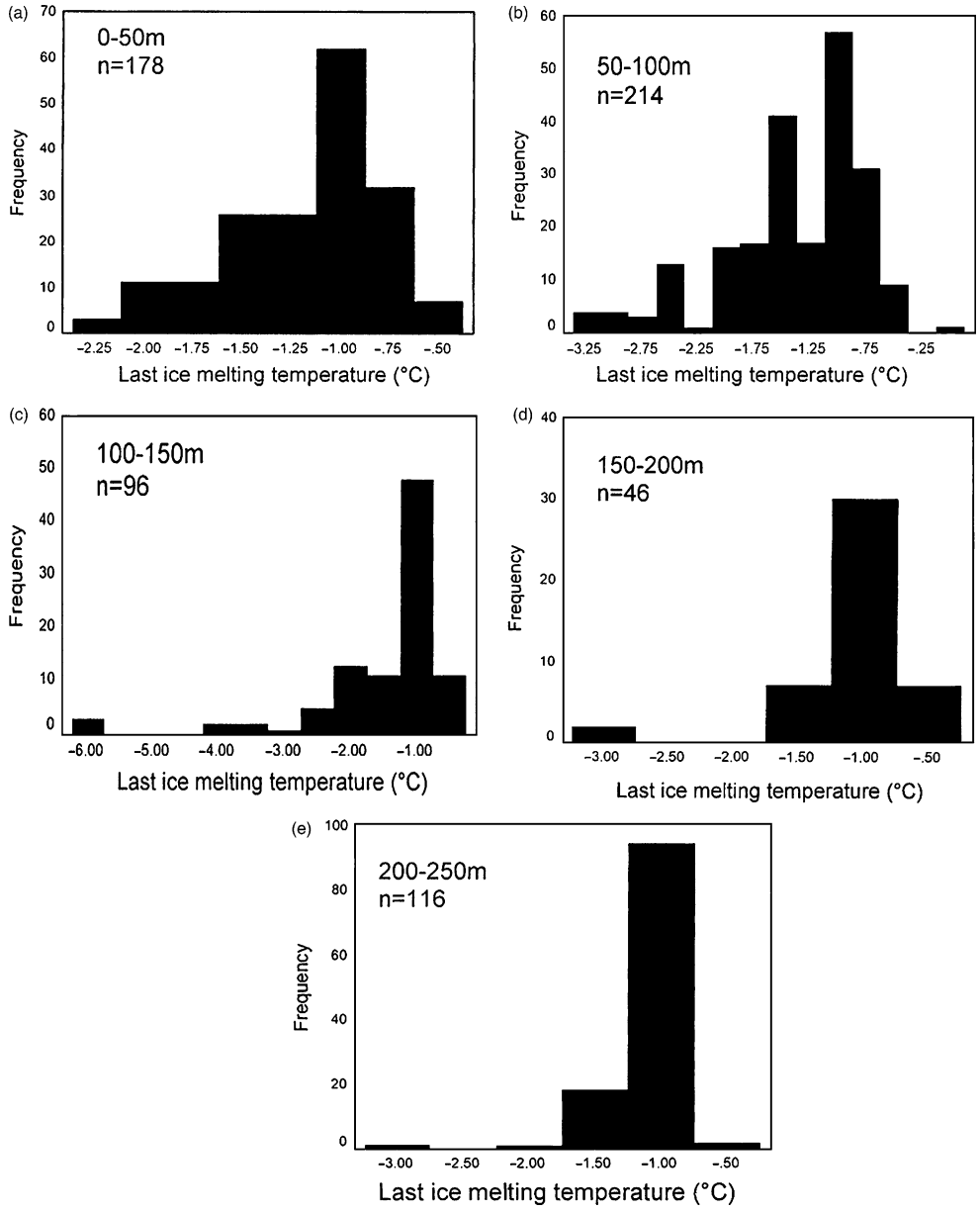

Fig. 9. Distribution of last ice-melting temperatures for aqueous two and three phases fluid inclusions at different depths: (a) at depths of 0–50 m; (b) at depths of 50–100 m; (c) at depths of 100–150 m; (d) at depths of 150–200 m; and (e) at depths of 200–250 m.

Table 1.
Oxygen stable isotope results (SMOW) obtained for quartz analyses from different horizons at the Qaleh-Zari deposit (below the present-day surface)

Sample no.	Depth (m bpds)	$\delta^{18}O_{quartz}$ (‰) (T=mean T_h)	$\delta^{18}O_{fluid}$ (‰) (T=280 °C)	$\delta^{18}O_{fluid}$ (‰)	Mean T_h (°C)
QZ6	0	6.7	−0.4	−0.9	294
QZ5	50	6.5	−1.8	−1.1	264
QZ8V1	100	6.5	−0.8	−1.1	288
QZ9V2	100	7.1	0.5	−0.5	308
QZ1V3	100	6.9	0.1	−0.7	303
QZ2	135	7.1	−1.3	−0.5	262
QZ3	170	7.3	−1.5	−0.3	253
QZ4	205	7.4	−0.7	−0.2	268
QZ7	240	7.5	0.0	−0.1	283

The $\delta^{18}O_{fluid}$ (SMOW) values are calculated at the same sample T_h mean and at the constant value 280 °C (total T_h mean). Calculated fluids use Matsuhisa et al. (1979).

deviation at one sigma) of the $\delta^{34}S$ for sulfide samples was $\pm 0.2‰$.

7. Discussion

7.1. Mineralizing processes

The microthermometric results, presented in Fig. 10a, and the low salinity of the fluid inclusions suggest that mineralization at Qaleh-Zari occurred under epithermal conditions (Hedenquist and Henley, 1985; Wilkinson, 2001). At Qaleh-Zari, as in most epithermal deposits, brecciation along fault planes at the commencement of mineralization permitted the introduction of a deep, multistage, circulating fluid into the ore-forming system. Hematite and quartz accompanied the commencement of each main mineralization stage and were followed by sulfosalt minerals, chalcopyrite and pyrite.

Vapor-rich fluid inclusions coexisting with the liquid+small-vapour inclusions in some samples and the homogenization of inclusions to the gaseous phase, indicate that boiling took place at some stage during mineralization (Drummond and Ohmoto, 1985; Plumlee, 1994; Simeone and Simmons, 1999; Ronacher et al., 2004). According to Scott and Watanabe (1998) the condensation of vapor in fractures from boiling accelerates the growth of quartz crystals with dusty, low-salinity fluid inclusion-rich margins. Coarse-grained and dusty quartz forms the center of most veins and is also found in the vugs at Qaleh-Zari. This evidence suggests boiling and followed by cooling were the important processes in ore precipitation within the Qaleh-Zari epithermal system (Scott and Watanabe, 1998; Ronacher et al., 2004) (Fig.10(b)).

7.2. Microthermometric data

Homogenization temperatures are plotted as histograms against depth and compared to the hydrostatic curve (Fig. 11), following Simmons (1991); Cooke and Simmons (2000).

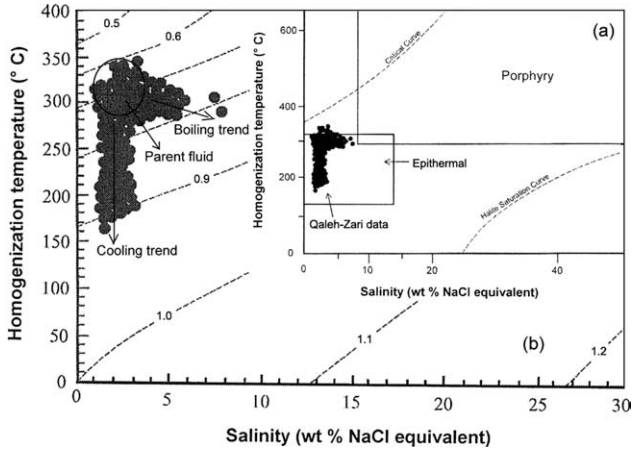

Fig. 10. Diagram showing homogenization temperatures for about 150 aqueous fluid inclusions against their salinity in quartz from different horizons at the Qaleh-Zari ore deposit: (a) The data plot in the epithermal zone; (b) Density diagram showing parent fluid, boiling trend and cooling trend (after Wilkinson, 2001).

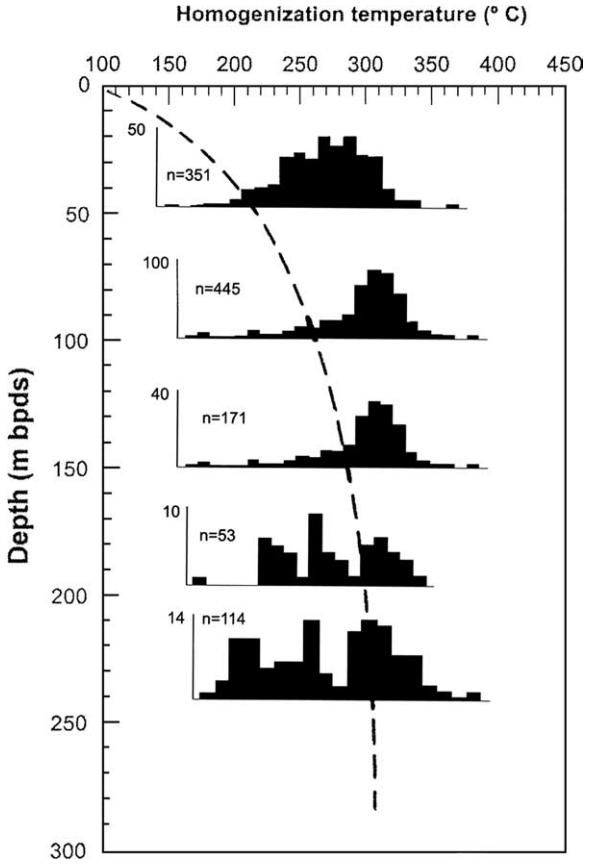

Fig. 11. Fluid inclusion temperature of homogenization data plotted in histograms as a function of depth compared to hydrostatic curve (after Cooke and Simmons, 2000).

Measurement of the last ice-melting temperature (T_m) and the homogenization temperature (T_h) were made on more than 145 fluid inclusions from the same samples at different horizons in the Qaleh-Zari deposit. Furthermore, salinities were calculated for these fluid inclusions using the equation of Bodnar (1993) for the H_2O–NaCl system (Table 2).

Dissolved CO_2 affects T_{mice} in a similar manner to dissolved salt. For inclusions with $T_{mice}(-2.5$ the lowering of the freezing point of water can be due to dissolved gas, not salt ($T_{mice}=-2.5$). Take for example pure water with dissolved CO_2—when this boils/degasses the residual liquid will have higher T_{mice} than the preboiled fluid. On the other hand a fluid with dissolved salt ($T_{mice}=-2.5$) will after boiling have lower T_{mice} than the parental fluid (Collins, 1979; Hedenquist and Henley, 1985; Diamond, 1992; Cooke and Simmons, 2000). Because, about 74.5% of measured fluid inclusions at the Qaleh-Zari deposit have T_{mice} between 0.0 to -1.5 °C. It is suggested, according to that the T_{mice} at this deposit could be due to the effects of dissolved gas, not salt (Hedenquist and Henley, 1985). Because the amount of the CO_2 phase was not measured in this study, salinity was calculated only for aqueous fluid inclusions. Probably, the CO_2 phase was derived from organic matter in sedimentary rocks, such as Jurassic shales, or from a magmatic volatile source (Vityk et al., 1994; Vallance et al., 2003; Ronacher et al., 2004).

Table 2.
Last ice melting temperatures (T_m), homogenization temperatures (T_h) and calculated salinity data for about 150 Type IV fluid inclusions in quartz collected from different horizons in the Qaleh-Zari deposit

Sample	T_m °C (*n*)	Salinity (*n*) wt% NaCl equiv	T_h °C (*n*)
Q.Z.S.	−1.4 to −1.5 (5)	2.4 to 2.6 (5)	245 to 310 (5)
Q.Z.S.	−2.0 to −2.1 (2)	3.0 to 3.1 (2)	290 to 293 (2)
L.50sf.7	−1.0 to −1.2 (3)	2.0 to 2.2 (3)	269 to 310 (3)
L.50sf.7	−0.6	1.5	276
Q.sf.6	−0.7 to −0.9 (7)	1.7 to 1.8 (7)	163 to 243 (7)
Q.sf.6	−1.0 to −1.3 (11)	2.0 to 2.3 (11)	205 to 305 (11)
Q.sf.6	−1.4 to −1.8 (6)	2.4 to 2.9 (6)	276 to 300 (6)
Q.sf.6	−2.0 to −2.8 (5)	3.0 to 4.0 (5)	300 to 319 (5)
Q.sf.6	−3.1 to −3.3 (4)	4.6 to 4.8 (4)	297 to 312 (4)
L.100w2	−0.8 to −1.0 (6)	1.7 to 2.0 (6)	285 to 303 (6)
L.135w2	−0.8 to −0.9 (4)	1.7 to 1.8 (4)	290 to 298 (4)
L.135w2	−1.0 to −1.7 (3)	1.8 to 2.8 (3)	290 to 306 (3)
L.170w2	−0.9 to −1.0 (5)	1.8 to 2.0 (5)	235 to 293 (5)
L.170w2	−0.5 to −0.8 (3)	1.4 to 1.7 (3)	199 to 239 (3)
L.205w2	−0.8 to −1.0 (9)	1.7 to 2.0 (9)	197 to 220 (9)
L.240w2	−0.7 to −1.0 (5)	1.6 to 1.8 (5)	179 to 231 (5)
L.240w2	−1.3 to −2.0 (3)	2.3 to 3.1 (3)	298 to 317 (3)
L.50sf.4	−0.5 to −0.7 (6)	1.4 to 1.6 (6)	209 to 308 (6)
L.50sf.4	−0.8 to −0.9 (12)	1.7 to 1.8 (12)	216 to 318 (12)
L.50sf.4	−1.0 to −1.2 (9)	2.0 to 2.4 (9)	213 to 320 (9)
L.50sf.4	−2.1 to −2.5 (2)	3.4 to 3.9 (2)	302 to 315 (2)
L.100sf.4	−0.5 to −0.9 (6)	1.4 to 1.8 (6)	238 to 300 (6)
L.100sf.4	−1.7 to −1.9 (5)	2.8 to 3.0 (5)	300 to 320 (5)
L.100sf.4	−2.5 to −2.8 (4)	3.7 to 4.1 (4)	286 to 320 (4)
L.100sf.4	−3.2	4.6	315
L.140sf.4	−1.0 to −1.8 (9)	2.0 to 3.0 (9)	188 to 325 (9)
L.140sf.4	−2.0 to −2.4 (4)	3.0 to 3.6 (4)	277 to 324 (4)
L.140sf.4	−3.3 to −3.8 (2)	4.7 to 5.3 (2)	302 to 306 (2)
L.140sf.4	−0.5 to −0.8 (9)	1.4 to 1.7 (9)	263 to 315(9)
L.140sf.4	−5.8	7.6	303

n: Number of measurements.

As it is indicated in Fig. 10b, a parental fluid with T_h about 300 °C and salinity $\leq$2 wt% NaCl equiv is envisaged for Qaleh-Zari system. A slight increase in the salinity occurred at about 300 °C, which was probably caused by boiling (Simmons and Browne, 1997; Cooke and Simmons, 2000). Fluid inclusions with low salinity ((3 wt% NaCl equiv) were probably trapped pre-boiling, while more saline fluid inclusions (3 wt% NaCl equiv) were trapped post- boiling (Scott and Watanabe, 1998). Fig. 10b shows that the density of mineralizing fluid at Qaleh-Zari ranged from 0.6 to 0.9 g cm^{-3}. We think that a slight increase in the density could be due to cooling and degassing (boiling) of the parental fluid.

7.3. Evolution and source of fluids

Considering the range of calculated $\delta^{18}O_{fluid}$ values from −1.8 to 0.5‰ (Table 1) a surface-derived fluid (because in this study δD was not measured, it is not possible to distinguish between meteoric and sea-water for this range of $\delta^{18}O$ values) can be proposed as the mineralizing fluid for the formation of the Qaleh-Zari deposit (Vallance et al., 2003). However, the mixing of magmatic volatiles with surficial waters cannot be ruled out. Also, in view of the narrow range of the measured $\delta^{18}O_{quartz}$ and calculated $\delta^{18}O_{fluid}$ values, the mineralizing fluid probably originated from a single source (Johnsen et al., 1996). Measured $\delta^{18}O_{quartz}$ values were plotted against sample depths (Fig. 12). This shows that $\delta^{18}O_{quartz}$ increases with depth. It is suggested that the slight difference in the $\delta^{18}O$ of quartz collected from different horizons of the Qaleh-Zari deposit is due to boiling (Moore et al., 1992; Plumlee, 1994). We think that quartz crystals precipitated from the parent fluid (pre-boiling and cooling) could be enriched with respect to $\delta^{18}O$.

The narrow range of measured $\delta^{34}S$ values (0.0–1.6‰) from the sulfide minerals at Qaleh-Zari suggests uniformity of the source region (Ohmoto and Rye, 1979; Canals and Cardellach, 1997; Baker et al., 2001). The samples have $\delta^{34}S$ values close to 0‰. So, these data suggest a magmatic origin for the sulfur in the Qaleh-Zari deposit (Vityk et al., 1994). Considering the volcanic nature of the host rocks at the Qaleh-Zari, sulfur is probably derived either by the leaching of primary sulfide minerals from volcanic host rocks or directly from a magmatic volatile source (Cooke and Simmons, 2000).

According to Cooke and Simmons (2000), in the Qaleh-Zari epithermal system, acidic-oxygenated surficial waters, after moving downwards and being heated by a deep-seated magmatic source, and with the addition of magmatic components, such as H_2O, CO_2, SO_2, H_2S, HCl, interacted with the wall-rocks, depositing hematite at high oxygen and low sulfur fugacities in the early stages of mineralization (Neal and Larson, 1994). However, at later stages as mineralization progressed, decreasing oxygen fugacity and increasing sulfur fugacity led to sulfide mineralization.

Evidence such as boiling, inclusions contained variable proportions of liquid and vapour and 'captive crystals' (trapped phases) all indicate the heterogeneous nature of the mineralizing fluid at the time of trapping (Shepherd et al., 1985; Prokofiev et al., 1999; Van den Kerkhof and Hein, 2001; Kilias et al., 2001). The ranges of salinity and density, and also the trapping temperatures of the fluid inclusions, indicate that boiling took place during various stages in the formation of the ore body at 160–1000 meters below the old water table,

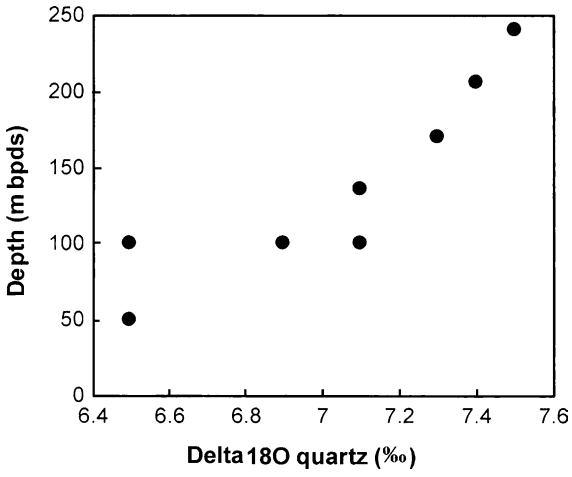

Fig. 12. Plot of sample depth versus $\delta^{18}O$ values from quartz samples collected from different horizons in the Qaleh-Zari deposit.

Table 3.
Comparison of the Qaleh-Zari deposit with other epithermal deposits in the world

Epithermal deposit	Host rock	Textures	Principal ore	Main gangue	Alteration	$\delta^{18}O$ ‰	T_h °C	Salinity. wt% NaCl equiv	Age of host
Qaleh-Zari Iran	Andesite basalt and andesitic tuffs	Open-Space filling and comb structures	Chalcopyrite Pyrite, Galena, Sphalerite, Hematite Electrum	Quartz, Calcite	Propylitic, Argillic, Phyllic	6.5–7.5 (quartz)	165–330	0.9 to 5	Tertiary
Waihi New Zealand[a]	Andesite	Fractures filling	Electrum, Acanthite, Pyrite, Sphalerite, Galena, Chalcopyrite	Quartz, Calcite	Propylitic, Argillic, K-Silicate	6.2–9.2 (quartz)	188–306	0.2 to1.7	Late Cenozoic
Shasta Canada[b]	Dacitic lapilli tuffs and Flows	Stockwork and replacement	Acanthite, Electrum, Native Silver, Galena Chalcopyrite, Sphalerite	Quartz, Calcite	Propylitic, Potassic, Sericitic	6.1 Average (quartz)	225–280	0 to 4	Jurassic
Lepanto Philipines[c]	Volcanic breccia, Dacite, Andesite	Breccia, Massive, Open-Space filling	Pyrite, Enargite, Luzonite, Tennantite, Chalcopyrite, Gold, Galena	Quartz, Anhdrite Barite	Advance argillic, K-silicate alteratio, Silica alteratio	7.8–10.9 (alunite)	200–300	2 to 4	Pliocene
Pajingo-Queensland[d]	Sandstones, Ignimbrite, Andesitic-volcanic	Crustification fracture filling	Pyrite, Sphalerite, Galena, Chalcopyrite, Electrum, Native gold hessite	Quartz, Calcite	Propylitic, Potassic, Argillic (intermediat)	4.7–7.88 (quartz)	170–315	0.7 to 2.5	Paleozoic

[a] Data from Brathwaite and Faure (2002).
[b] Data from Thiersch et al. (1997).
[c] Data from Hedenquist et al. (1998).
[d] Data from Bobis et al. (1995)

at pressures between 15 and 80 bars (Haas, 1971). Evidence, such as hydraulic fracturing and brecciation in veins, suggests that an overpressured hydrothermal fluid was active during some of the mineralization stages (Ronacher et al., 2004).

Some of characteristics of the Qaleh-Zari deposit, such as host rocks, textures, ore and gangue minerals, alteration, range of $\delta^{18}O$, T_h, salinity and age of host rocks are compared with other epithermal deposits in the world in Table 3.

8. Conclusions

Mineralization at Qaleh-Zari was controlled by structures, such as fault and breccia zones. Textures in the breccias can be identified as tectonic (pre-mineralization) or hydrostatic (syn-mineralization). Ore microscopy and field observations show that there were several pulses of mineralizing fluid, with steep pressure and temperature gradients, resulting in the telescoping of the ore zone and the deposition of a profusion of mineral species in some parts of Qaleh-Zari.

The petrography of the fluid inclusions indicates that ore deposit at Qaleh-Zari is zoned with respect to depth, as indicated by:

1. The occurrence of liquid-rich and vapor-rich fluid inclusions in the deeper parts of the system.
2. The absence of Vapor-rich inclusions in the upper levels of the system.

Considering the estimated range of hydrostatic pressure (15–80 bars) within Qaleh-Zari system, boiling probably occurred either in an open or a closed system (Simmons and Browne, 1997). Hydrostatic brecciation in early ore minerals and coexisting liquid- and vapor-rich fluid inclusions in the same samples indicate that at about 1 km depth, with decreased permeability, boiling occurred in a closed system (adiabatic). Trapping of liquid-rich fluid inclusions and steam-loss at shallow depth indicate that with increasing permeability (faults and brecciated zones), boiling occurred in an open system (non-adiabatic) (Simmons and Browne, 1997; Scott and Watanabe, 1998).

Based on criteria presented by Hedenquist et al. (2000); Sillitoe and Hedenquist (2003); Cooke and Simmons (2000) for low-, intermediate- and high-sulfidation, and considering texture and structures, alteration, T_h, salinity, ore and gangue minerals and the host rocks, the deposit at Qaleh-Zari can be classified as a low-sulfidation style ore body.

According to experimental data and field observations it may be said that boiling, cooling and wall-rock interactions were the main controlling factors in the formation of the Qaleh-Zari ore deposit.

Acknowledgements

The authors would like to thank the Managing Director of the Minakan Company for his help during the fieldwork. Dr Tony Fallick, the director of Scottish Universities

Environmental Research Center in Scotland, is thanked for his much appreciated isotopic analyses. Dr Jonathan Naden (BGS, Keyworth), Dr Jeremy Richards (University of Alberta) and Dr David Alderton (University of London) are thanked for reviewing and making critical comments on the original manuscript.

References

Baker, T., Perkins, C., Blake, K.L., Williams, P.J., 2001. Radiogenic and stable isotope constraints on the genesis of the Eloise Cu–Au deposit, Cloncurry district northwest Queensland. Economic Geology 96, 723–742.

Bazin, D., Hubner, H., 1969. Copper deposits in Iran. Geological Survey of Iran, Internal Report No. 13, p. 195 (in English).

Bobis, R.E., Jaireth, S., Morrison, G.W., 1995. The anatomy of a Carboniferous epithermal ore shoot at Pajingo, Queensland; setting, zoning, alteration, and fluid conditions. Economic Geology 90, 1776–1798.

Bodnar, R.J., 1993. Revised equation and table for determining the freezing point depression of H_2O–NaCl solution. Geochimica et Cosmochimica Acta 57, 683–684.

Brathwaite, R.L., Faure, K., 2002. The Waihi epithermal gold–silver-base metal sulfide–quartz vein system, New Zealand: temperature and salinity controls on electrum and sulfide deposition. Economic Geology 97, 269–290.

Canals, A., Cardellach, E., 1997. Ore lead and sulfur isotope pattern from the low-temperature veins of the Catalonian Coastal Ranges (NE Spain). Mineralium Deposita 32, 243–249.

Collins, P.L.F., 1979. Gas hydrates in CO_2-bearing fluid inclusions and the use of freezing data for estimation of salinity. Economic Geology 74, 1435–1444.

Cooke, D.R., Simmons, S.F., 2000. Characteristics and genesis of epithermal gold deposits. In: Hagemann, S.G., Brown, P.E. (Eds.), Gold in 2000 Reviews in Economic Geology, vol. 13, pp. 221–244.

Daymehvar, M., 1996. Study of geology, mineralogy, geochemistry and genesis of Qaleh-Zari copper deposit. Unpublished MSc Thesis. Teacher Training University, p. 133 (in Farsi).

Diamond, L.W., 1992. Stability of CO_2 clathrate hydrate + CO_2 liquid + CO_2 vapour + aqueous KCl–NaCl solutions: experimental determination and application to salinity estimates of fluid inclusions. Geochimica et Cosmochimica Acta 56, 273–280.

Drummond, S.E., Ohmoto, H., 1985. Chemical evolution and mineral deposition in boiling hydrothermal systems. Economic Geology 80, 126–147.

Hassan-Nezhad, A.A., 1994. Geochemical and fluid inclusion studies at the Qaleh-Zari Copper Mine, Khorasan Province, Iran. Unpublished MSc Thesis. Shiraz University, Shiraz, p. 216 (in Farsi).

Hass Jr., J.L., 1971. The effect of salinity on the maximum thermal gradient of a hydrothermal system at hydrostatic pressure. Economic Geology 66, 940–946.

Hedenquist, J.W., Henley, R.W., 1985. The importance of CO_2 on freezing-point measurements of fluid inclusions—evidence from active geothermal systems and implications for epithermal ore deposition. Economic Geology 80, 1379–1406.

Hedenquist, J.W., Arribas, A.R., Reynolds, T.J., 1998. Evolution of an intrusion-centered hydrothermal system: Far Southeast-Lepanto porphyry and epithermal Cu–Au deposits, Philippines. Economic Geology 93, 373–404.

Hedenquist, J.W., Arribas, A.R., Gonzalez-Urien, E., 2000. Exploration for epithermal gold deposits. In: Hagemann, S.G., Brown, P.E. (Eds.), Gold in 2000 Reviews in Economic Geology, vol. 13, pp. 245–277.

Johnsen, C.A., Cardellach, E., Tritlla, J., Hanau, B.B., 1996. Circa Pb–Zn–Ag vein deposits: isotopic and fluid inclusion evidence for formation during the Mesozoic extension in the Pyrenees of Spain. Economic Geology 91, 506–997.

Joseph, G., 1999. Copper, its Trade, Manufacture, use and Environmental Status. Society for Metals Press, 451p.

Karimpour, M.H., Zaw, K., 2000. Geothermometry and physicochemical condition of Qaleh-Zari Cu–Au ore bearing solution based on chlorite composition and fluid inclusion study. Iranian Journal of Crystallography and Mineralogy 8, 3–22 (in Farsi with English abstract).

Khatib, M.M., 1999. The relationship between shear strain and ore-bearing veins at the Qaleh-Zari mine. In: Proceedings of Mineral Potential of East Iran, pp. 70–71 (in Farsi).

Khoie, N., Qorbani, M., Tajbakhsh, P., 1999. Copper deposits in Iran. Geological Survey of Iran Press, 421p. (in Farsi).

Kilias, S.P., Naden, J., Cheliotis, I., Shepherd, T.J., Constandinidou, H., Crossing, J., Simos, I., 2001. Epithermal gold mineralization in the active Aegean Volcanic Arc: the Profitis Ilias deposit, Milos Island, Greece. Mineralium Deposita 36, 32–44.

Macaulay, C.I., Fallick, A.E., Hazeldine, R.S., Graham, C.M., 2000. Methods of laser-based stable isotope measurement applied to diagenetic cements and hydrocarbon reservoir quality. Clay Minerals 35, 313–322.

Matsuhisa, Y., Goldsmith, J.R., Clayton, R.N., 1979. Oxygen isotopic fractionation in the system quartz–albite–anorthite–water. Geochimica et Cosmochimica Acta 43, 1131–1140.

Moore, F., Hassan-Nezhad, A.A., 1994. Fluid inclusion study of mineralization at the Qaleh-Zari Mine, South Khorasan, Iran. Iranian Journal of Science and Technology 18, 213–223.

Moore, J.N., Adams, M.C., Lemieux, M.M., 1992. The formation and distribution of CO_2-enriched fluid inclusions in epithermal environments. Geochimica et Cosmochimica Acta 56, 121–135.

Neal, W.S., Larson, P.B., 1994. Mineral and fluid geochemistry of the Hoosier Vein, Chloride Mining District, Sierra County, New Mexico. Economic Geology 89, 1752–1768.

Ohmoto, H., Rye, R.O., 1979. Isotopes of sulfur and carbon. In: Barnes, H.L. (Ed.), Geochemistry of Hydrothermal Ore Deposits, second ed. Wiley, New York, pp. 509–567.

Plumlee, G.S., 1994. Fluid chemistry evolution and mineral deposition in the Main-Stage Creede epithermal system. Economic Geology 89, 1860–1882.

Prokofiev, V., Sikamenetsky, V., Kovalenker, V., Bodon, S.B., Jelen, S., 1999. Evolution of magmatic fluid at the Banska Stiavnica precious and base metal deposit, Slovakia—evidence from melt and fluid inclusions. Economic Geology 94, 949–956.

Roedder, E., Roedder, E., 1984. Fluid Inclusions, Reviews in Mineralogy 12. Mineralogical Society of America, 646p.

Ronacher, E., Richards, J.P., Reed, M.H., Bray, C.J., Spooner, E.T.C., Adams, P.D., 2004. Characteristics and evolution of the hydrothermal fluid in the North Zone high-grade area, Porgera Gold Deposit, Papua New Guinea. Economic Geology 99, 843–867.

Sadaghyani-Avval, F., 1976. Etude géologique de la région de la mine de Khal-Eh-Zari (Iran) mineralisation et inclusions fluids. Unpublished PhD Thesis, Université de Nancy, Nancy, p. 165.

Scott, A.M., Watanabe, Y., 1998. 'Extreme boiling' model for variable salinity of the Hokko low-sulfidation epithermal Au prospect, southwestern Hokkaido, Japan. Mineralium Deposita 33, 568–578.

Shepherd, T.J., Rankin, A.H., Alderton, D.H.M., 1985. A Practical Guide to Fluid Inclusion Studies. Blackie Press, 239 p.

Sillitoe, R.H., Hedenquist, J.W., 2003. Linkages between volcanotectonic settings, ore-fluid compositions and epithermal precious-metal deposits. In: Simmons, S.F., Graham, I. (Eds.), Volcanic, Geothermal, and Ore-forming fluids: Rulers and Witnesses of Processes within the Earth. Society of Economic Geologists Special Publication, 10, pp. 315–343.

Simeone, R., Simmons, S.F., 1999. Mineralogical and fluid inclusion studies of low-sulfidation epithermal veins at Osilo (Sardinia), Italy. Mineralium Deposita 34, 705–717.

Simmons, S.F., 1991. Hydrologic implications of alteration and fluid inclusion studies in the Fresnillo district, Mexico: evidence for a brine reservoir and a descending water table during the formation of hydrothermal Ag–Pb–Zn ore bodies. Economic Geology 86, 1579–1601.

Simmons, S.F., Browne, P.R.L., 1997. Saline fluid inclusions in sphalerite from the Broadlands–Ohaaki geothermal system: a coincidental trapping of fluids being boiled toward dryness. Economic Geology 92, 485–489.

Suzuki, Y., Ogawa, K., Akiyama, N., 1976. Copper ores from the Qaleh-Zari Mine, Iran. Mining Geology 385, 26–391.

Thiersch, P.C., Williams-Jones, A.E., Clark, J.R., 1997. Epithermal mineralization and ore controls of the Shasta Au–Ag deposit, Toodoggone district, British Columbia, Canada. Mineralium Deposita 32, 44–57.

Vallance, J., Cathelineau, M., Boiron, M.C., Fourcade, S., Shepherd, T.J., Naden, J., 2003. Fluid–rock interactions and the role of late Hercynian aplite intrusion in the genesis of the Castromil gold deposit, northern Portugal. Chemical Geology 194, 201–224.

Van den Kerkhof, A.M., Hein, U.F., 2001. Fluid inclusion petrography. Lithos 55, 27–47.

Vityk, M.O., Krouse, H.R., Skakun, L.Z., 1994. Fluid evolution and mineral formation in the Beregovo gold-base metal deposit, Transcarpathia, Ukraine. Economic Geology 89, 547–565.

Wilkinson, J.J., 2001. Fluid inclusions in hydrothermal ore deposit. Lithos 55, 229–272.